Spinodal decomposition of polymer solutions: A parallelized molecular dynamics simulation

Leonid Yelash, Peter Virnau, Wolfgang Paul, and Kurt Binder
Institut für Physik, Johannes Gutenberg-Universität Mainz, Germany

Marcus Müller
Institut für Theoretische Physik, Georg-August-Universität Göttingen, Friedrich-Hund-Platz 1, 37077 Göttingen, Germany

(Received 25 April 2008; published 5 September 2008)

In simulations of phase separation kinetics, large length and time scales are involved due to the mesoscopic size of the polymer coils, and the structure formation on still larger scales of length and time. We apply a coarse-grained model of hexadecane dissolved in supercritical carbon dioxide, for which in previous work the equilibrium phase behavior has been established by Monte Carlo methods. Using parallelized simulations on a multiprocessor supercomputer, large scale molecular dynamics simulations of phase separation following pressure jumps are presented for systems containing $N=435\,136$ coarse-grained particles, which correspond to several millions of atoms in a box with linear dimension 447 Å. Even for large systems the phase separation can be observed up to the final, macroscopically segregated, equilibrium state. It is shown that in the segregation process the two order parameters of the system (density and concentration) are strongly coupled. The system does not follow the predicted growth law for the characteristic domain size $\ell(t) \propto t$ in binary fluid mixtures for the range of times accessible in the simulation. Instead, it exhibits a distinctly slower growth, presumably due to the dynamic asymmetry of the constituents.

DOI: 10.1103/PhysRevE.78.031801 PACS number(s): 61.25.he, 61.20.Ja, 61.20.Lc, 64.75.Jk

I. INTRODUCTION

Kinetics of phase separation in binary mixtures is a key process for pattern formation in various solids and liquids [1–5]. Understanding these processes is a fundamental problem of nonequilibrium statistical mechanics, and also relevant for many industrial processes, e.g., the production of polymeric foams [6–11]. In the latter case, a key aspect of the problem is the strong dynamic asymmetry between the constituents, giving rise to special effects known as "viscoelastic phase separation" [12]: The polymer melt resulting from the phase separation process has a viscosity that is orders of magnitude larger than that of the solvent. The solvent can be a dense gas, like in the case of supercritical carbon dioxide, which is often used in this process [9–11] and in many related pattern formation processes [13–15].

It is generally believed that in binary fluid mixtures, which are essentially symmetric in their intrinsic dynamic properties (such as fluid mixtures of small molecules, see [1–5] for examples), the growth of the linear dimension $\ell(t)$ with time t after the system was quenched from the one-phase region into the two-phase region (by a temperature or pressure jump) can be described by simple power laws

$$\ell(t) \propto t^a. \tag{1}$$

The growth mechanisms are therefore determined by the corresponding values of the growth exponent a, which can be understood theoretically [1–5,16–21]. In addition, there is evidence [1–5] that the equal-time structure factor $S(q,t), q$, being the wave number of the scattering, satisfies a simple scaling property in the late stages

$$S(q,t) = [\ell(t)]^d \tilde{S}[q\ell(t)], \quad d = \text{system dimensionality}. \tag{2}$$

Explicit predictions for the scaling function $\tilde{S}$ exist [3,22–25]. However, for viscoelastic phase separation neither Eq. (1) nor (2) seem to hold, and the behavior observed experimentally appears to be far more complex [12].

In the present paper, we discuss a feasibility study of simulating the phase separation of a simple atomistic model of a polymer solution with molecular dynamics (MD) [26–28] methods. Previous work on MD simulation of phase separation kinetics has either addressed the liquid-vapor transition of simple fluids (e.g., Ref. [29]) or binary mixtures of simple fluids (e.g., Ref. [30]). Phase separation studies of symmetric polymer blends by Monte Carlo methods of lattice models [31,32] do neither include hydrodynamic effects nor a dynamic asymmetry between the species. We are mainly interested in atomistic models within which we can make an explicit connection to a specific system. Therefore, we disregard numerical studies of phenomenological coarse-grained models in this context such as lattice Boltzmann simulations [33], dissipative particle dynamics [34] models, or numerical solutions [35] of "model H" [36].

The starting point of our study is a coarse-grained model [37–40] for a short polymer (hexadecane) dissolved in carbon dioxide (Sec. II). For this model, both the static phase diagram has been explored, and also information on the interfacial tension between coexisting phases is available [39,40]. In order to be able to study large enough systems over large enough time scales, the application of a multiprocessor supercomputer is mandatory. Section III reports on the implementation of our problem with use of the MD simulation package ESPResSo [41–43]. Section IV describes typical results for the observed time evolutions during phase separation for this model. Some conclusions are summarized in Sec. V.

II. A COARSE-GRAINED MODEL FOR HEXADECANE-CARBON-DIOXIDE MIXTURES

Although hexadecane ($C_{16}H_{34}$) is an oligomer rather than a long polymer, its fully atomistic simulation with an all-

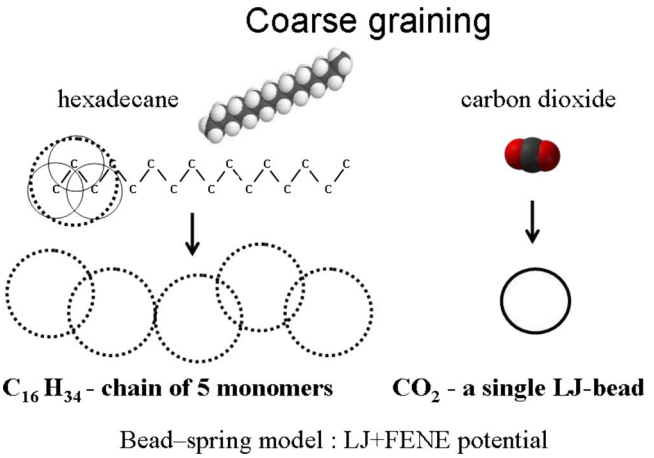

FIG. 1. (Color online) Illustration of the coarse-graining procedure: In the case of hexadecane, three successive C-C bonds are integrated into one bead (dotted circle). The oligomer, containing 50 atoms (or 16 united atoms of CH_3 or CH_2, respectively) is thus reduced to an effective chain of five monomers. Neighboring effective monomers along a chain interact with a combination of Lennard-Jones (LJ) and finitely extensible nonlinear elastic (FENE) potentials; nonbonded particles interact with a single LJ potential only. Carbon dioxide is represented by a single Lennard-Jones bead.

atom model under melt conditions is a difficult task, because large length and time scales need to be explored to describe spinodal decomposition. Thus, we coarse grain the model for this molecule by incorporating three successive C-C bonds along a chain (plus the corresponding H atoms) into one effective bead. Hexadecane is therefore described by a chain of five effective monomers (Fig. 1). Effective monomers along a chain are bonded together via FENE (finitely extensible nonlinear elastic) springs [44]

$$U_{\mathrm{FENE}}(r) = -33.75\varepsilon_{\mathrm{pp}} \ln[1-(r/R_{\mathrm{pp}})^2], \quad R_{\mathrm{pp}} = 1.5\sigma_{\mathrm{pp}}. \tag{3}$$

$\varepsilon_{\mathrm{pp}}, \sigma_{\mathrm{pp}}$ are the parameters of the Lennard-Jones potential which acts between all beads of the chains (bonded as well as nonbonded ones),

$$U_{\mathrm{LJ}}(r) = \begin{cases} 4\varepsilon_{\alpha\beta}[(\sigma_{\alpha\beta}/r)^{12} - (\sigma_{\alpha\beta}/r)^6 + 127/16\,384], & r < r_{\mathrm{cut}}, \\ 0, & r \geqslant r_{\mathrm{cut}}, \end{cases} \tag{4}$$

with a cutoff $r_{\mathrm{cut}} = 2\sqrt[6]{2}\sigma_{\alpha\beta}$. Here, $\alpha, \beta = p$ if the particle is an effective monomer of the polymer chain or $\alpha, \beta = s$ in case of a solvent particle, respectively. The parameters $\varepsilon_{\mathrm{pp}}, \sigma_{\mathrm{pp}}$ and $\varepsilon_{\mathrm{ss}}, \sigma_{\mathrm{ss}}$ are fixed by the requirement that the experimental critical temperatures T_c and densities ρ_c of $C_{16}H_{34}$ and CO_2 are reproduced [38–40]. Note that for $C_{16}H_{34}$ [45], $T_c = 723$ K and $\rho_c = 0.219$ g/cm^3. Modeling these values with the corresponding critical temperature and density as obtained from the simulations of 5-mers [38–40], we identify

$$\varepsilon_{\mathrm{pp}} = 5.79 \times 10^{-21} J, \quad \sigma_{\mathrm{pp}} = 4.52 \times 10^{-10} m. \tag{5}$$

From now on, $\varepsilon_{\mathrm{pp}}$ and σ_{pp} will be taken as our units of temperature and length (and the index p will be omitted). From the critical parameters $T_c = 304$ K, $\rho_c = 0.464$ g/cm^3 of CO_2 and computer simulations of Lennard-Jones monomers [38–40] we deduce

$$\varepsilon_{\mathrm{ss}} = 0.726\varepsilon, \quad \sigma_{\mathrm{ss}} = 0.816\sigma. \tag{6}$$

With these parameters [Eqs. (5) and (6)] the coexistence curves and vapor pressures at coexistence of the pure components can be reproduced reasonably well over a wide temperature regime [39]. We also obtain a good description of the temperature dependence of the interfacial tension between coexisting phases [38–40]. A significantly better description of CO_2 is obtained when one includes the quadrupole-quadrupole interaction [46]. However, this very recent extension of our model is not considered here.

We still need to determine $\varepsilon_{\mathrm{ps}}, \sigma_{\mathrm{ps}}$ describing the effective interactions between CO_2 molecules and the effective beads of the polymer. The standard assumption for such a problem is the Lorentz-Berthelot mixing rule [47]

$$\sigma_{\mathrm{sp}} = (\sigma_{\mathrm{ss}} + \sigma_{\mathrm{pp}})/2, \quad \varepsilon_{\mathrm{sp}} = \sqrt{\varepsilon_{\mathrm{ss}}\varepsilon_{\mathrm{pp}}}. \tag{7}$$

However, it has turned out [39,40] that Eq. (7) yields a rather unsatisfactory description of the phase diagram of the mixed system $CO_2 + C_{16}H_{34}$. In order to reproduce the correct phase diagram type and obtain rough agreement with experiment [48,49], one must introduce a parameter ξ describing deviations from the Lorentz-Berthelot rule,

$$\varepsilon_{\mathrm{sp}} = \xi\sqrt{\varepsilon_{\mathrm{ss}}\varepsilon_{\mathrm{pp}}}, \quad \xi = 0.886. \tag{8}$$

Figure 2(a) shows a projection of the resulting phase diagram into the pressure-temperature plane. Figure 2(b) describes an isothermal slice through the phase diagram in the plane of variables pressure p and mole fraction $x = n_s/(n_s + n_p)$ with n_s and n_p being the number of molecules of solvent and polymer, respectively. In this diagram, also the pressure jump quenching experiment and the resulting time evolution of the system is indicated. Note that for a mole fraction $x = 0.6$ of CO_2, the prediction for the spinodal curve as derived from perturbation theory [39] would imply that phase separation starts by nucleation and growth. The pressure jump indicated in Fig. 2(b) leads to a state in between the coexistence curve and spinodal curve. However, this is not true. Although, TPT1-MSA gives a reliable prediction for the thermodynamic properties of the phases coexisting in equilibrium, one should not attach much quantitative significance to its prediction of the spinodal curve. The actual transition between nucleation and spinodal decomposition occurs much closer to the coexistence curve as indicated in Ref. [50]. Hence, the initial state after the quench is instantaneously thermodynamically unstable. Concentration and density inhomogeneities form everywhere in the system, as discussed in more detail in Sec. IV.

III. SIMULATION DETAILS AND IMPLEMENTATION CONSIDERATIONS

For our simulations, we use the ESPResSo package, version 1.9.7h, 2005 [41,42]. Newton's equations of motion are

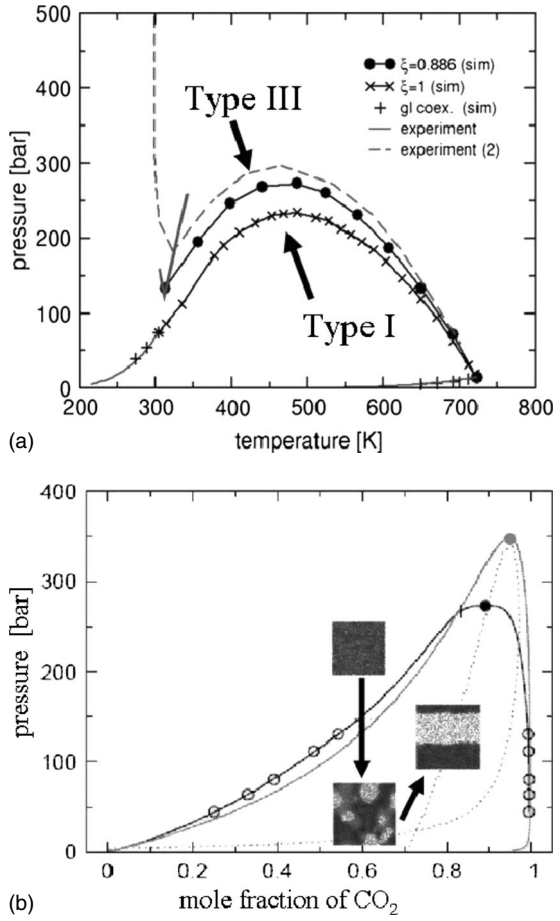

FIG. 2. (a) Projection of the critical line of the polymer +solvent mixture into the pressure-temperature plane (parameter changing along the curve is the mole fraction x of CO_2). For $\xi=1$ [Eq. (7)], this line starts out for $x=0$ at the critical point of $C_{16}H_{34}$ at $T_c=723$ K by construction, reaches a maximum pressure at about $T_{\max}=486$ K, and then the critical pressure decreases again and reaches the critical point of CO_2 (so-called "type I" phase diagram). For $\xi=0.886$ [Eq. (8)], however, the critical curve rather reaches a minimum at $T_{\min}\approx 315$ K, in agreement with experiment [48]. For the pure systems the vapor pressures at vapor-liquid coexistence are also shown (including the experimental data [45]). From Ref. [39]. (b) Isothermal slice through the phase diagram at $T_{\max}=486$ K ($T^*=1.16$), showing the coexistence curve between the polymer-rich phase (left) and CO_2 supercritical vapor (near $x=1$, right), both according to the Monte Carlo calculation and from thermodynamic perturbation theory (TPT1-MSA) [39]. The prediction of the spinodal curve resulting from TPT1-MSA is shown as a dotted curve. Note that the TPT1-MSA overestimates the critical pressure, but yields an accurate prediction of the coexistence curve at low pressures. The small snapshot pictures of slices through the simulation box connected by arrows indicate the quenching experiment and the resulting structure evolution in the systems. The initial density and pressure (in Lennard-Jones units) were $\rho^*=0.8$ and $p^*=0.34$, while the final state was $\rho^*=0.45$ and $p^*=0.12$ (at $t=4000\tau$). These reduced pressures correspond to $p=213$ bar and $p=75.2$ bar, respectively.

integrated with a velocity Verlet algorithm and a time step $\Delta t=0.002\tau$. The MD time unit τ is defined as $\tau=\sigma(m/\varepsilon)^{1/2}$. Here, the mass $m=1$, for simplicity, irrespective of whether we consider a CO_2 molecule or an effective monomeric unit. Choosing different masses proportional to the actual molecular masses, would enhance the dynamic asymmetry only slightly. Indeed, the MD time unit calculated using Eq. (5) and the average molar mass of a hexadecane bead $m_p=45.2$ g/mol is $\tau_p\approx 1.63$ ps, whereas using Eq. (6) and the molar mass of carbon dioxide $m_s=44$ g/mol one obtains $\tau_s\approx 1.54$ ps. In view of the coarse-grained character of the model this complication is disregarded here.

In our simulations, we work with as many as $N=435\,136$ effective particles (CO_2 molecules or beads resulting from the coarse graining in Fig. 1). Recall that $C_{16}H_{34}$ and CO_2 are mapped to only five and one effective monomers, respectively, which implies that we simulate a system containing several millions of atoms. The initial state is chosen to be a homogeneous solution at reduced density $\rho^*\equiv\rho\sigma^3=0.8$, temperature $T^*\equiv k_BT/\varepsilon=1.16$, and pressure $p^*\equiv p\sigma^3/\varepsilon=0.34$ (in LJ units, which correspond to $T=486$ K and $p=213$ bar). After the density jump to $\rho^*\equiv\rho\sigma^3=0.45$ [or associated increase of volume of the system by the factor of 1.78 from $L^3=(81.6\sigma)^3$ to $L^3=(98.88\sigma)^3$], the systems were simulated in microcanonical ensemble up to the final equilibrium state with two planar interfaces between the coexisting phases. The reduced equilibrium pressure of this state was $p^*=0.12$ ($p=75.2$ bar) and the box linear dimension corresponds to 447 Å after the quench.

Creating a well equilibrated initial state of such a polymer solution with manageable computational effort is in itself a challenging task. Hence, we followed here a similar strategy as has been applied to a related study of spinodal decomposition in confined polymer solutions [43]. On a single-CPU PC, we create a small and well-equilibrated system with a box of linear dimension $L/\sigma=20.4$ containing $N'=6799$ particles, which we then replicate four times in each direction to $L/\sigma=81.6$. Of course, the initial state will still have a structure which reflects the periodic boundary condition with $L/\sigma=20.4$. This fact shows up indeed when we consider the equal-time structure factors, which for a binary (AB) system are defined as follows. The number density structure factor is [51]

$$S_{\rm nn}(q)=S_{AA}(q)+S_{BB}(q)+2S_{AB}(q), \tag{9}$$

while the structure factor measuring correlations in the relative concentration is defined as

$$S_{\rm cc}(q)=x_B^2S_{AA}(q)+x_A^2S_{BB}(q)-2x_Ax_BS_{AB}(q), \tag{10}$$

Finally, cross correlations between density and concentration need to be considered, too,

$$S_{\rm nc}(q)=x_BS_{AA}(q)-x_AS_{BB}(q)+(x_B-x_A)S_{AB}(q). \tag{11}$$

The partial structure factors $S_{\alpha\beta}(\alpha,\beta=A,B)$ are defined as

$$S_{\alpha\beta}(q)=\frac{1}{N}\sum_{k=1}^{N_\alpha}\sum_{\ell=1}^{N_\beta}\langle\exp[i\vec{q}\cdot\vec{r}_{k\ell}]\rangle,\quad \vec{r}_{k\ell}=\vec{r}_k-\vec{r}_\ell. \tag{12}$$

Figure 3 shows, e.g., the structure factors involving the concentration, $S_{\rm cc}(q)$ and $S_{\rm nc}(q)$. In both structure factors, one sees a "Bragg peak" at $q_{\min}=2\pi/(20.4)\approx 0.308$, reflecting that initially the large system exhibits the periodicity re-

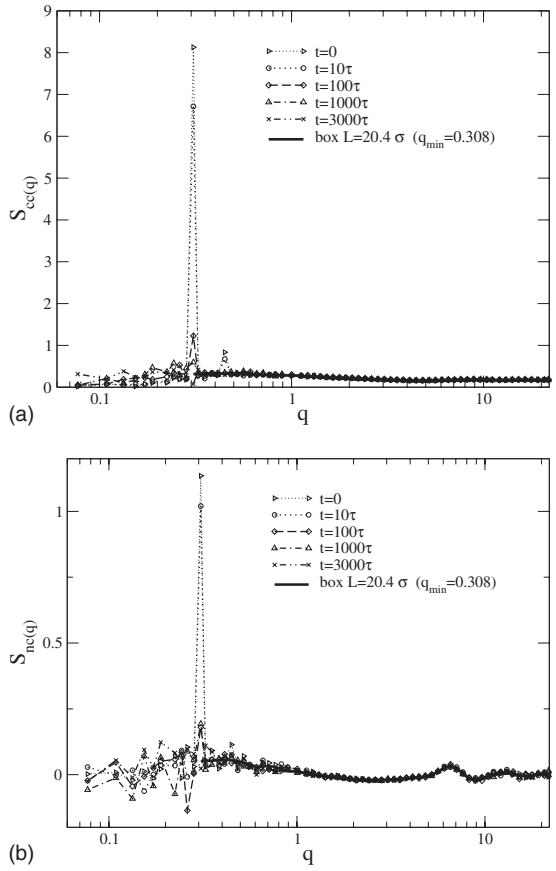

FIG. 3. (a) Concentration-concentration structure factor $S_{cc}(q)$ and (b) concentration-density structure factor $S_{nc}(q)$ plotted vs wave vector q on a logarithmic scale, for $L/\sigma=81.6$, $\rho^*=0.8$, $x=0.6$, and $T^*=1.16$. The dotted curves, which exhibit the sharp maximum at $q=q_{min}=0.308$ (i.e., the minimum wave number for the small box with $L/\sigma=20.4$), represents the structure shortly after replication ($t=0$ and $t=10\tau$), while the dashed-dotted curves represents the final structure after 1000 and 3000 MD time steps without such peaks. For comparison, the structure factor at an intermediate time of equilibration (after 100 MD time steps, dashed curve) is also included, as well as the structure factors recorded for the initial small box with the box length 20.4σ (solid curve).

sulting from the fact that we start from a periodic arrangement of 64 identical smaller boxes. However, this periodicity is quickly lost in the subsequent equilibration run of the large box. Note that due to the large size of the system (containing $N=435\,136$ particles), this run is already carried out in parallel on up to 128 CPUs of the IBM-p960 multiprocessor supercomputer (JUMP) of the John von Neumann-Institute for Computing (NIC) in Jülich. We use the geometric domain decomposition scheme, which is implemented in the ESPResSo software [41,42] and enables an efficient parallelization of our systems.

The smallest wave number for large systems is $q_{min}/4=0.077$, but one should note that only 6 wave vectors $\vec{q}[(q_{min}/4)(\pm 1,0,0);(q_{min}/4)(0,\pm 1,0);(q_{min}/4)(0,0,\pm 1)]$ contribute to the results for $S_{\alpha\beta}(q)$ for this smallest wave number. Since $S_{\alpha\beta}(\vec{q})$, where $\vec{q}$ is treated as a vector, is not self-averaging [52], there is an inevitable problem of statistical accuracy: The relative accuracy of an average of $S_{\alpha\beta}(\vec{q})$, recorded from $\mathcal{N}$ statistically independent observations, is independent of the size of the simulation box and decreases with increasing $\mathcal{N}$ only as [52] $\sqrt{2/\mathcal{N}}$. In Fig. 3, $S_{cc}(q)$ and $S_{nc}(q)$ is not averaged over observations at different times. At small $|\vec{q}|$, we average only over the wave vectors $\vec{q}$ that have exactly the same absolute value $|\vec{q}|$. While for large $|\vec{q}|$, many wave vectors contribute and, hence, a reasonable accuracy is reached. Therefore, for the smallest possible wave number $q_{min}/4$ (to which only six wave vectors contribute) the resulting accuracy is rather poor. For wave numbers that are only slightly larger (such as $\sqrt{2}q_{min}/4$, $\sqrt{3}q_{min}/4$, $2q_{min}/4$, etc.), the situation is similar. However, Fig. 3 does imply that in the q range where the initial Bragg peak appeared at $q_{min}=2\pi/(20.4)$, a rather short run suffices to wipe out this periodicity. We emphasize this point since when the simulation of the quenching experiment is performed, a peak in $S_{nn}(q)$ and $S_{cc}(q)$ occurs at small q, and this growth of fluctuations would be seriously affected if periodicity was already present there.

It is also interesting to note that $S_{nc}(q)$ exhibits pronounced peaks at $q=7$, $q=14$, etc., while in $S_{cc}(q)$ such peaks are absent. Similar peaks occur in the density-density structure factor $S_{nn}(q)$ shown in Fig. 4. These peaks are expected, of course, as they reflect the packing of particles at distances comparable to σ in a dense fluid [53]. This structure is independent of the size of the box.

When we examine the behavior of $S_{cc}(q)$ and $S_{nn}(q)$ at small q (i.e., $q<1$), we notice an increase with decreasing q, compatible with Ornstein-Zernike behavior [53],

$$S_{nn}(q)=S_{nn}(0)/(1+q^2\xi_{nn}^2), \quad S_{cc}(q)=S_{cc}(0)/(1+q^2\xi_{cc}^2). \tag{13}$$

Both static "susceptibilities" $S_{nn}(0)$, $S_{cc}(0)$, are of the same order $S_{nn}(0)\approx 0.236$, $S_{cc}(0)\approx 0.34$ and also the correlation lengths are of the same order, and rather small $\xi_{nn}\approx\xi_{cc}\approx 0.5$. This indicates that the initial state is quite homogeneous, neither long-range density fluctuations nor long-range concentration fluctuations are present.

Figure 4 shows the change of both $S_{nn}(q)$ and $S_{cc}(q)$ when the pressure jump (or associated volume expansion, respectively) is performed. While Fig. 4(b) implies that practically no significant changes occur in $S_{cc}(q)$, the splitting of the first peak in $S_{nn}(q)$ after the quench indicates that the sudden expansion of the box does affect the intermolecular packing significantly. In the regime $1\leqslant q\leqslant 5$ there is also a strong enhancement of $S_{nn}(q)$. We interpret this finding as an implication that the quench does disturb the local equilibrium significantly. This finding was unexpected and not intended. Indeed, we expected smaller deviations from local equilibrium. Since local equilibrium needs to be reestablished before the scaling and universality concepts outlined in Eqs. (1) and (2) can be applied meaningfully, we will remove the first 10 MD time units from the analysis. These short times will just reflect the path of the system back towards local equilibrium.

IV. TIME EVOLUTION OF THE PHASE SEPARATION IN THE HEXADECANE-CARBON-DIOXIDE MIXTURES

Figure 5 presents a series of snapshot pictures, indicating the onset of spinodal decomposition, which leads to the

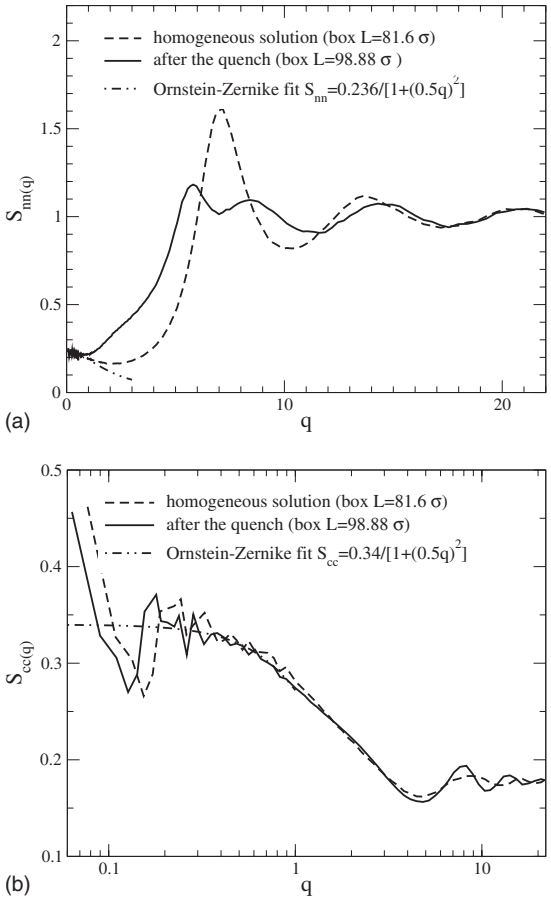

FIG. 4. (a) Density-density structure factor $S_{nn}(q)$ after equilibration in the large box ($L/\sigma=81.6$) and immediately after the quench where the volume of the box has increased to $L/\sigma=98.88$. Data refer to $x=0.6$, $\rho^*=0.8$, and $T^*=1.16$, as in Fig. 3. (b) Same as (a) but for the concentration-concentration structure factor $S_{cc}(q)$. Note that although we averaged over 10 runs, the statistics for $q<0.3$ is still poor. The Ornstein-Zernike behavior quoted in the text applies to the range $0.3 \leqslant q \leqslant 1$.

spontaneous growth of both density fluctuations and concentration fluctuations. The initial state is homogeneous on large scales, as it should be, but it contains small-scale fluctuations of both density and concentration, compatible with our discussion of the corresponding structure factors (Fig. 4). One can see that soon after the quench ($t=10\tau$) an almost periodic arrangement of density and concentration inhomogeneities has formed. There are "gas bubbles," which contain empty space and some CO_2 molecules with in between dissolved isolated polymer chains [e.g., as shown in the inset of Fig. 5(c)]. Much CO_2 seems to have moved from the interior of the polymer-rich percolating background to the interfaces between polymer and vapor. Note that the vapor phase also forms a spongelike percolating structure throughout the box similar to the polymer-rich phase due to the chosen conditions where in the final state [Fig. 5(e)] the volume fraction of both phases is comparable. Indeed, in Fig. 5(d) one can see two mutually percolating domains of both phases in $d=3$ dimensions where the CO_2-rich phase (gray domains) appears near the corners of the box and the polymer-rich phase (black domains) fills the remaining space of the box.

In the later stages (e.g., $t=1000\tau$), as well as in the equilibrium slablike structure [Fig. 5(e)] where two planar interfaces are connected into themselves via the periodic boundary condition, we can observe a few polymer chains dissolved in the (supercritical) carbon-dioxide gas. The density of dissolved CO_2 molecules in the $C_{16}H_{34}$ matrix is clearly smaller than the gas density in the vapor phase, as expected. However, we shall not discuss further the behavior of such equilibrium interfaces here, but rather defer this to a later presentation [54].

Here, we are concerned with the structure factors and their time evolution (Fig. 6). Note that Fig. 6 shows "raw data" from which we get a honest impression about the statistical accuracy of our original simulation data. While 10 independent runs were averaged over, no averaging over some time intervals Δt was performed. In addition to the averaging over independent systems, we also do coarse-graining over some wave-number intervals $\Delta \log_{10}(q)$ by distributing 30 intervals (bins) homogeneously per one decade of the q axis on the logarithm scale. As expected from our discussion of the corresponding data in equilibrium, the statistical accuracy is very good for large q due to the large number of vectors $\vec{q}$ that typically contribute to the same $|\vec{q}|$ and also due to many closely located $|\vec{q}|$ that can be accumulated into the same q intervals. For small $q<0.2$, however, due to increasing distance between $|\vec{q}|$ and decreasing number of vectors, larger statistical inaccuracy is present, as expected.

While $S_{nn}(q,t)$ shows structure at large q, $S_{cc}(q,t)$ at large q does not show any significant structure. Neither of these structure factors shows a significant time dependence at large q, too. While the pattern of the density and concentration distributions (Fig. 5) change rapidly with time, local equilibrium is rapidly established on the small scales representing nearest-neighbor correlations in the system. Remarkably, although the packing in the final equilibrium state [Fig. 5(e)] differs clearly between both coexisting phases due to their different total densities, this does not show up in the "Lennard-Jones (LJ) peak" seen in $S_{nn}(q,\tau)$.

The peak representing spinodal decomposition is already very well developed at $t=10\tau$ (Fig. 6) both in $S_{nn}(q,\tau)$ and in $S_{cc}(q,\tau)$, and shifts distinctly with increasing time to smaller q, indicating that the coarsening stage sets in almost immediately after the quench. Thus, there is no regime of times visible where the structure factor grows, exponentially increasing with time, and the peak occurs at the same position without shifting to smaller q, as the linearized theory of spinodal decomposition would predict [1,4]. This failure of the linear theory is expected, of course: The Ginzburg criterion [55] implies that the linearized theory holds for the initial stages in symmetrical polymer blends in the limit of very large molecular weight, and this prediction is compatible with experiments [2,4] and simulation [32]. For polymer solutions, however, nonlinear effects are already important during the early states of the growth of fluctuations, and this is compatible with the present observations.

Figure 7 presents a log-log plot of a characteristic domain scale $\ell(t)$ vs time, which we define here using the first moment of the distribution $S_{nn}(q)$,

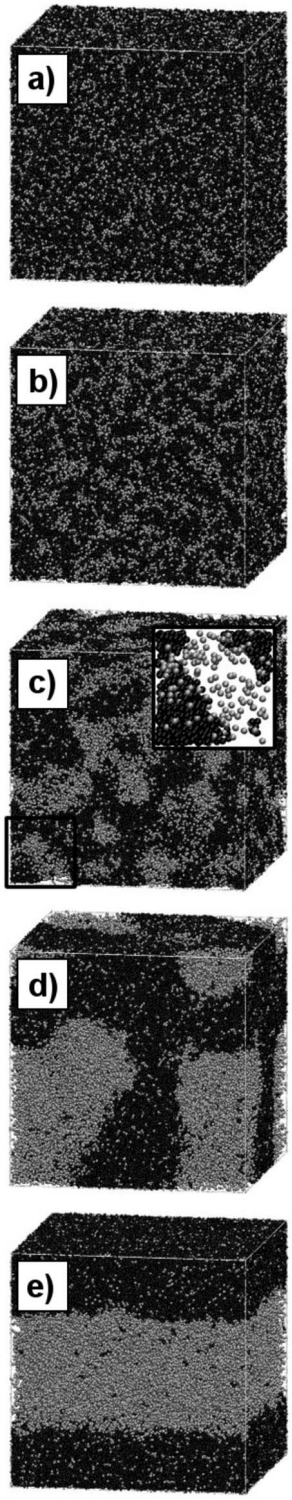

FIG. 5. Snapshot pictures illustrating the time evolution as recorded in our simulation of a quenching experiment. Times shown are (a) $t=0$ (the initial state before the quench), (b) $t=10\tau$, (c) $t=100\tau$, (d) $t=1000\tau$, and (e) $t=4000\tau$. The inset in (c) shows an enlarged region of size $20\times20\times5\sigma^3$ marked by the rectangle at the left-bottom corner: Gray spheres represent the solvent molecules (CO_2); dark spheres are the effective beads of $C_{16}H_{34}$. One oligomer contains five such beads. For clarity no bonds connecting these beads are shown. The white background represents empty space ("free volume").

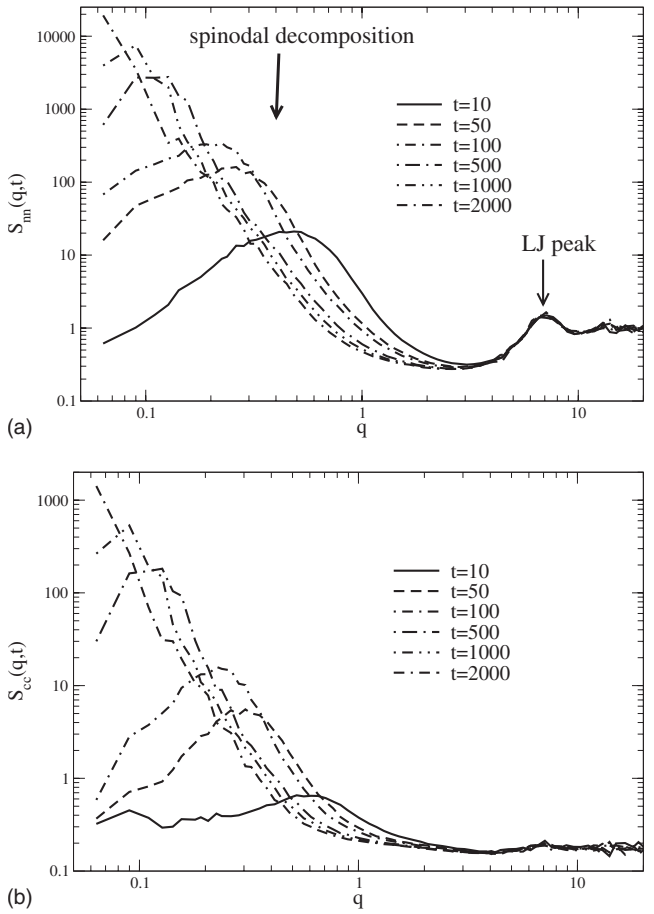

FIG. 6. (a) Equal-time density-density structure factor $S_{nn}(q,t)$ and (b) concentration-concentration structure factor $S_{cc}(q,t)$ on a log-log plot vs wave vector q. Different curves show times from $t=10\tau$ to $t=2000\tau$ after the quench, as indicated. The 10 independent runs were averaged over.

$$\ell(t) = 2\pi \sum_{q=0}^{q_{\rm cut}} S_{\rm nn}(q,t) \Bigg/ \sum_{q=0}^{q_{\rm cut}} q S_{\rm nn}(q,t), \qquad (14)$$

where for the cutoff $q_{\rm cut}$ we use values $q_{\rm cut}=1$, 3, and 5. Note that the minimum of $S_{\rm nn}(q,t)$ occurs at $q_{\rm cut}\approx3$. For $t\geqslant30$, the scale $l(t)$ becomes practically independent of the cutoff. An alternative measure of $l(t)$ would be the inverse of the peak position, $2\pi/q_{\rm max}(t)$, but due to the statistical inaccuracy $q_{\rm max}(t)$ cannot be estimated with high accuracy for small q and large t from our data. The inset in Fig. 7 shows the slope of the curves $\log_{10}(l)$ on $\log_{10}(t)$, which can be understood as an effective (t-dependent) exponent a used in Eq. (1). We calculate the slope by differentiating numerically our data $a_i=\frac{\log_{10}(l_{i+2}/l_i)}{\log_{10}(t_{i+2}/t_i)}$ and centering a_i at $t_c=\sqrt{t_i t_{i+2}}$.

From Fig. 7 we observe that the growth of $\ell(t)$ sets in at very early times, and a power law $\ell(t)\propto t^{1/3}$ is compatible with the data for $100\leqslant t\leqslant1000$, i.e., for one decade to which we have fitted the dotted-dashed line and obtained the slope $a=0.333\pm0.003$. Then, a crossover to a faster growth occurs, which for $t\leqslant2000$ is compatible with another power law, $\ell(t)\propto t^{0.45}$. From the inset in Fig. 7 one can also see that the effective exponent $a(t)$ oscillates between 0.25 and 0.4

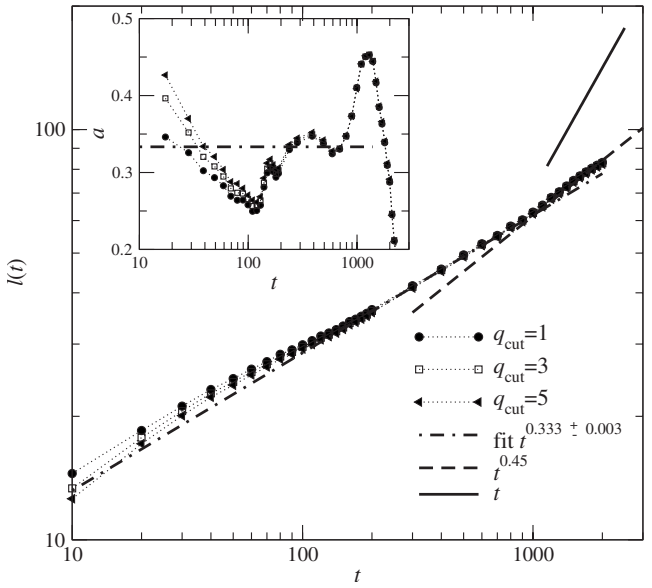

FIG. 7. Log-log plot of the characteristic domain linear dimension $\ell(t)$ vs time for three different values of cutoff q_{cut}, as illustrated, cf. Eq. (14). Straight lines illustrate the power laws for different exponents: $\ell(t) \propto t^{0.333}$ was obtained by fitting the data for $q_{\mathrm{cut}}=5$ in range of t from 100τ to 1000τ, $\ell(t) \propto t^{0.45}$ and $\ell(t) \propto t$ are shown to guide the eyes. The inset shows the slope of the curves [an effective exponent $a(t)$] obtained by numerical differentiation of data $a_i = \frac{\log_{10}(l_{i+2}/l_i)}{\log_{10}(t_{i+2}/t_i)}$ and centering a_i at $t_c = \sqrt{t_i t_{i+2}}$. For $t > 1000\tau$, $a(t)$ decreases very rapidly due to finite size effects in our simulations.

for early time and increases systematically above $a=1/3$ for $t > 800\tau$. However, $a(t)$ drops down very rapidly beyond $t \approx 1000\tau$ due to finite system size effects: $\ell(t)$ bends off and seems to saturate in this regime.

Experience with slow crossovers in related plots of experimental data [1,4], where more decades in time and length are available, show, however, that typically the crossover from one power law to another is spread out over several decades in time. Thus, it is rather doubtful that the asymptotic regime of Eqs. (1) and (2) has actually been reached in Fig. 7. In fact, the scaling property postulated in Eq. (2) can only be verified rather roughly with the present data.

In the context of simulations of spinodal decomposition for Ising lattice models of binary mixtures [56], it was shown that it may be advantageous to analyze the correlation function $G_{\mathrm{cc}}(r,t)$ of concentration fluctuations, rather than its Fourier transform $S_{\mathrm{cc}}(q,t)$. Hence, we have recorded such radial distribution functions as well. As an example, Fig. 8 presents the shifted particle-particle radial distribution function $g(r,t)-1$ of the effective monomers of hexadecane at various times. One can see that there always occur rapid oscillations at small distances ($r \leqslant 3$), reflecting the typical packing of spherical particles in a dense fluid. $g(r,t=0)-1$ is essentially zero for $r > 3$ expressing the fact that the fluid in the initial equilibrium is homogeneous on these scales. After the quench one sees a long-range correlation building up. Unlike the case of critical fluctuations, where the correlation function is non-negative, we see that at large distances during the phase separation kinetics, the particle-particle radial

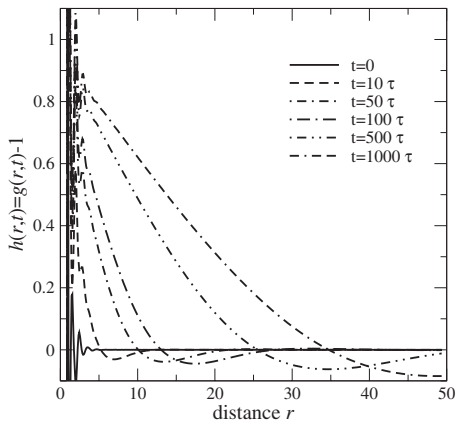

FIG. 8. Time evolution of the radial distribution function between the effective hexadecane units for different times, as indicated. The intersections of these curves with $g(r,t)=1$ for $r > 3$ are identified with a characteristic domain scale $l_2(t)$ shown in Fig. 9.

distribution function $g(r,t)-1$ actually crosses zero and changes sign. This zero crossing can be taken [43,56] as a second measure of the characteristic length scale of spinodal decomposition, $l_2(t)$. For $r \geqslant l_2(t)$, it is likely that one has crossed an interface between a $C_{16}H_{34}$-rich domain and a CO_2-rich domain. Unlike the case of critical quenches in the Ising model [56], where a perfect symmetry between both coexisting phases exists, in our system the minimum of $g(r,t)$ is very shallow, however.

In Fig. 9 we show a log-log plot of this length scale $l_2(t)$ versus time as well as an effective exponent $a_2(t)$ calculated for $l_2(t)$ in the same way as we calculated $a(t)$ for $l(t)$ in Fig. 7. The behavior of $l_2(t)$ [and $a_2(t)$] qualitatively is similar to that of $l(t)$ [and $a(t)$] in Fig. 7: Initially, an increase of $l_2(t)$ proportional to $t^{\approx 0.36}$; for $100 < t < 1000$, the increase of $l_2(t)$

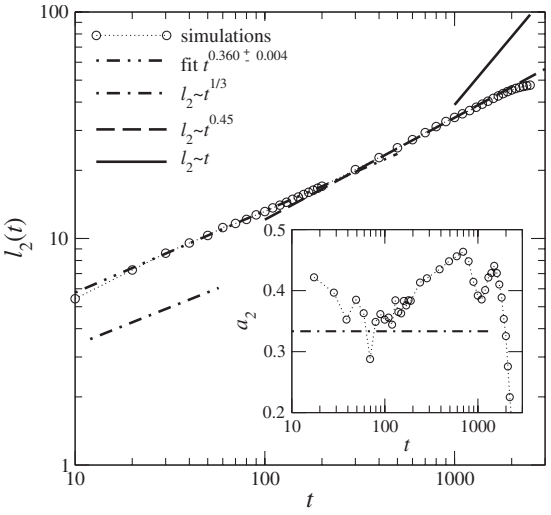

FIG. 9. Log-log plot of the characteristic domain linear dimension $\ell_2(t)$ vs time calculated from the radial distribution function $g(r,t)$. Also, power laws for exponent $a_2=0.36$, which was obtained by fitting data in the range of t from 30τ to 300τ, as well as for $a_2=1/3$, 0.45, and 1 are shown to guide the eyes. The inset shows an effective exponent $a_2(t)$ vs time obtained by numerical differentiation of data in the same way as $a(t)$ in Fig. 7.

changes to $t^{\approx 0.45}$, and then the finite size effects limit the further growth. However, one should note that the scales of $l_2(t)$ and $l(t)$ are quantitatively still different [roughly $l(t) \approx 2l_2(t)$].

For approximately symmetric binary fluid mixtures, one expects a power law $l(t) \propto t^{1/3}$ for strongly off-critical quenches due to the diffusion and coagulation of droplets [1–5,17], while for critical quenches hydrodynamic flow along the interfaces causes asymptotically a faster growth, $l(t) \propto t$ [1–5,18]. However, it should be noted that $l(t)$ must grow by several orders of magnitude, in order that its growth law $l(t) \propto t$ can be observed clearly [2,4]. Hence, our system is clearly still too small to reach this regime.

V. CONCLUSIONS AND OUTLOOK

In the present work, spinodal decomposition in a compressible, asymmetric polymer solution following a sudden volume expansion of the system was simulated. The underlaying coarse-grained model (Fig. 1) reproduces the phase behavior of hexadecane+carbon-dioxide mixtures in thermal equilibrium (Fig. 2). Using the ESPResSo software in a parallel implementation on a multiprocessor, we can follow the phase separation kinetics from the initial stage up to completion (Fig. 5) for a system containing $N=435\,136$ coarse-grained particles (effective monomers or CO_2 molecules, respectively). Our coarse graining implies that we simulate a system containing several millions of atoms, and the box linear dimension corresponds to 447 Å after the quench. Recall also that $C_{16}H_{34}$, which contains 50 atoms, is mapped to only five effective monomers. We find that there is no regime of physically meaningful time where the linearized Cahn-Hillard theory of spinodal decomposition is applicable. The coarsening behavior starts immediately after the quench. Very roughly, this coarsening can be described in terms of a power law for the length scale $l(t)$ [or $l_2(t)$] that characterizes the size of the growing phase separated domains, which, however, does not exhibit a unique growth exponent. Instead, the latter depends on the range of times that is studied, and the precise definition used to measure the length scale. Furthermore, the finite size effects limit the structure growth in our systems for $t > 1000\tau$. However, such difficulties are rather common in systems undergoing spinodal decomposition.

The present system is particularly interesting, since both density and composition fields, which initially are both homogeneous, develop large-scale inhomogeneities in the course of the quench. Carbon-dioxide-rich vapor bubbles form, that contain hardly any polymers, while the polymer-rich regions have only a small fraction of carbon dioxide dissolved. Such an interplay of two variables, density and mole fraction in our case, is very common in the processing applications of polymer solutions. Our simulation is a first step towards the computational modeling of such processes.

Unfortunately, a direct comparison of our simulations to experiments is not possible, since the time scales studied by us are clearly in the submicrosecond range, while in the laboratory quenching experiments can only be carried out on much larger time scales. Although, it would be very desirable to study spinodal decomposition with a model of a polymer solution containing many millions of coarse-grained particles over a time interval at least one order of magnitude longer than we studied here, we concluded that this task would have been impractical with the given grant of CPU time. However, we hope that the insight into these very early stages of phase separation will stimulate further theoretical work using mesoscale models, and also guide the interpretation of experiments that study much larger scales of length and time.

ACKNOWLEDGMENTS

We are grateful to the John von Neumann Institute for Computing (NIC) for a grant of computer time on the JUMP multiprocessor and to the EU Network of Excellence for access to the SOFTCOMP Cluster at Jülich Supercomputing Centre. We thank T. Stühn for his advice on the ESPResSo software package. S.K. Das and J. Horbach are acknowledged for helpful discussions.

[1] J. D. Gunton, M. San Miguel, and P. S. Sahni, in *Phase Transitions and Critical Phenomena*, edited by C. Domb and J. L. Lebowitz (Academic, London, 1983), Vol. 8, p. 267.
[2] *Dynamics of Ordering Processes in Condensed Matter*, edited by S. Komura and H. Furukawa (Plenum, New York, 1988).
[3] A. J. Bray, Adv. Phys. **43**, 357 (1994).
[4] K. Binder and P. Fratzl, in *Phase Transformations in Materials*, edited by G. Kostorz (Wiley-VCH, Weinheim, 2001), p. 409.
[5] A. Onuki, *Phase Transition Dynamics* (Cambridge University Press, Cambridge, 2002).
[6] R. M. Hikmet, S. Callister, and A. Keller, Polymer **29**, 1378 (1988).
[7] J. H. Han and C. D. Han, J. Polym. Sci., Part B: Polym. Phys. **28**, 711 (1990).
[8] S. K. Goel and E. J. Beckman, Polym. Eng. Sci. **34**, 1137 (1994).
[9] C. M. Stafford, T. P. Russell, and T. J. McCarthy, Macromolecules **32**, 7610 (1999).
[10] B. Krause, H. J. P. Mettinkhof, N. F. A. van der Vegt, and M. Wessling, Macromolecules **34**, 874 (2001).
[11] B. Krause, J. H. J. P. Sijbesma, P. Mününklü, N. F. A. van der Vegt, and M. Wessling, Macromolecules **34**, 8792 (2001).
[12] H. Tanaka, J. Phys.: Condens. Matter **12**, R207 (2000).
[13] R. Butler, C. M. Davies, and A. I. Cooper, Adv. Mater. (Weinheim, Ger.) **13**, 1459 (2001).
[14] A. I. Cooper, Adv. Mater. (Weinheim, Ger.) **13**, 1111 (2001).
[15] *Supercritical Carbon Dioxide in Polymer Reaction Engineering*, edited by M. F. Kemmere and Th. Meyer (Wiley-VCH, Weinheim, 2005).
[16] I. M. Lifshitz and V. V. Slyozov, J. Phys. Chem. Solids **19**, 35 (1961).

[17] K. Binder and D. Stauffer, Phys. Rev. Lett. **33**, 1006 (1974).
[18] E. D. Siggia, Phys. Rev. A **20**, 595 (1979).
[19] M. San Miguel, M. Grant, and J. D. Gunton, Phys. Rev. A **31**, 1001 (1985).
[20] H. Furukawa, Phys. Rev. A **31**, 1103 (1985); Adv. Phys. **34**, 703 (1985).
[21] H. Furukawa, Phys. Rev. A **36**, 2288 (1987).
[22] H. Furukawa, Physica A **123**, 497 (1984).
[23] C. Yeung, Phys. Rev. Lett. **61**, 1135 (1988).
[24] P. Fratzl, J. L. Lebowitz, O. Penrose, and J. Amar, Phys. Rev. B **44**, 4794 (1991).
[25] G. F. Mazenko, Phys. Rev. E **58**, 1543 (1998).
[26] M. P. Allen and D. J. Tildesley, *Computer Simulation of Liquids* (Clarendon, Oxford, 1987).
[27] D. C. Rapaport, *The Art of Molecular Dynamics Simulation* (Cambridge University Press, Cambridge, 1995).
[28] *Monte Carlo and Molecular Dynamics of Condensed Matter*, edited by K. Binder and G. Ciccotti (Italian Physical Society, Bologna, 1996).
[29] S. W. Koch, R. C. Desai, and F. F. Abraham, Phys. Rev. A **27**, 2152 (1983); R. Yamamoto and K. Nakanishi, Phys. Rev. B **49**, 14958 (1994); **51**, 2715 (1995); H. Kabrede and R. Hentschke, Physica A **361**, 485 (2005).
[30] W. J. Ma, A. Maritan, J. R. Banavar, and J. Koplik, Phys. Rev. A **45**, R5347 (1992); M. Laradji, S. Toxvaerd, and O. G. Mouritsen, Physica A **239**, 404 (1997); Phys. Rev. Lett. **77**, 2253 (1996).
[31] A. Sariban and K. Binder, Macromolecules **24**, 578 (1991).
[32] E. Reister, M. Müller, and K. Binder, Phys. Rev. E **64**, 041804 (2001).
[33] V. M. Kendon, M. E. Cates, I. Pagonabarraga, J.-C. Desplat, and P. Bladon, J. Fluid Mech. **440**, 147 (2001); F. J. Alexander, S. Chen, and D. W. Grunau, Phys. Rev. B **48**, 634 (1993); S. Chen and T. Lookman, J. Stat. Phys. **81**, 223 (1995).
[34] P. B. Warren, Phys. Rev. Lett. **87**, 225702 (2001).
[35] T. Koga and K. Kawasaki, Phys. Rev. A **44**, R817 (1991); S. Puri and B. Dünweg, *ibid.* **45**, R6977 (1992); O. T. Valls and J. E. Farrell, Phys. Rev. E **47**, R36 (1993); A. Shinozaki and Y. Oono, *ibid.* **48**, 2622 (1993).
[36] P. C. Hohenberg and B. I. Halperin, Rev. Mod. Phys. **49**, 435 (1977).
[37] P. Virnau, M. Müller, L. G. MacDowell, and K. Binder, Comput. Phys. Commun. **147**, 378 (2002).
[38] P. Virnau, M. Müller, L. G. MacDowell, and K. Binder, New J. Phys. **6**, 7 (2004).
[39] P. Virnau, M. Müller, L. G. MacDowell, and K. Binder, J. Chem. Phys. **121**, 2169 (2004).
[40] K. Binder, M. Müller, P. Virnau, and L. G. MacDowell, Adv. Polym. Sci. **173**, 1 (2005).
[41] This package is available at the homepage http://www.espresso.mpg.de
[42] H.-J. Limbach, A. Arnold, B. A. Mann, and C. Holm, Comput. Phys. Commun. **174**, 704 (2006).
[43] K. Bucior, L. Yelash, and K. Binder, Phys. Rev. E **77**, 051602 (2008).
[44] K. Kremer and G. S. Grest, J. Chem. Phys. **92**, 5057 (1990).
[45] NIST website: http://webbook.nist.gov/chemistry/
[46] B. M. Mognetti, L. Yelash, P. Virnau, W. Paul, K. Binder, M. Müller, and L. G. MacDowell, J. Chem. Phys. **128**, 104501 (2008).
[47] G. C. Maitland, M. Rigby, E. B. Smith, and W. A. Wakeham, *Intermolecular Forces* (Clarendon, Oxford, 1981).
[48] C. T. Amon, R. J. Martin, and R. Kobayashi, Fluid Phase Equilib. **31**, 89 (1986).
[49] G. Schneider, Z. Alwani, W. Heim, E. Horvath, and E. U. Franck, Chem.-Ing.-Tech. **39**, 649 (1967).
[50] M. Müller, L. G. MacDowell, P. Virnau, and K. Binder, J. Chem. Phys. **117**, 5480 (2002).
[51] A. B. Bhatia and D. E. Thornton, Phys. Rev. B **2**, 3004 (1970).
[52] A. Milchev, K. Binder, and D. W. Heermann, Z. Phys. B: Condens. Matter **63**, 521 (1986).
[53] J. P. Hansen and I. R. McDonald, *Theory of Simple Liquids* (Academic, London, 1986).
[54] L. Yelash, P. Virnau, W. Paul, K. Binder, and M. Müller (unpublished).
[55] K. Binder, J. Chem. Phys. **79**, 6387 (1983).
[56] J. G. Amar, F. E. Sullivan, and R. D. Mountain, Phys. Rev. B **37**, 196 (1988).